Ninth International Conference on Computational Fluid Dynamics (ICCFD9), Istanbul, Turkey, July 11-15, 2016

ICCFD9-2016

LES-IB computations of flows with large temperature and density variations

Artur Tyliszczak, Mariusz Ksiezyk, Witold Elsner

Department of Mechanical Engineering and Computer Science
Czestochowa University of Technology, Poland

Corresponding author: atyl@imc.pcz.pl

Abstract: This paper presents a solution algorithm for Large Eddy Simulations-Immersed Boundary (LES-IB) approach for laminar/turbulent flows with large temperature and density variations. The proposed algorithm is based on the projection method and low Mach number approximation. The IB method is implemented in a variant of direct forcing. The time integration is performed using a predictor-corrector approach and the spatial discretization is based on high-order compact schemes on half-staggered meshes. The accuracy and stability of the proposed method is verified in 2D/3D simulations of the flow around cylinder and sphere. A comparison with the solution obtained using a body-fitted approach shows very good agreement of the obtained results. The LES-IB is then applied for computations of 3D turbulent flow in a wavy channel. We analyze an influence of wall shape on heat exchange and we study how the waviness parameters (amplitude, frequency) affect the flow behaviour, the Nusselt number and a pressure drop.

Keywords: Low Mach Number Flows, Turbulent Flows, Immersed Boundary Method.

1 Introduction

Large eddy simulation (LES) method gives very deep inside into physical flow behaviour and provides detailed information on both steady and unsteady flow phenomena. On an academic ground LES is often used with precise high-order compact and spectral/pseudospectral methods, which use is limited to rather simple computational geometries and also by boundary conditions enforced by the type of the method (eg. periodic boundaries for Fourier method). The easiest solution which allows using of the compact methods in complicated domains and/or with solid objects in the flow domains is to combine them with the Immersed Boundary (IB) method. Advantage of the IB method over the classical approach with body-fitted meshes is that the flows can be solved on Cartesian grids and the objects immersed in the flow domain can be arbitrarily complex as there is no need to design the mesh around. It was demonstrated that IB method can be successfully applied together with the spectral methods [1] and finite/compact difference methods [2, 6, 7], as well as in the context of LES applications [3, 4, 5]. Recently, the IB method has been applied for low Reynolds number laminar flows with small density variations, i.e. within the Boussinesq approximation [8]. In the present paper we extend the IB approach to low Mach number turbulent flows with density/temperature differences in the range $1-5$. We apply the IB method in combination with the solution algorithm formulated in [9, 10]. We focus on development of the LES-IB approach, its verification and then application in a complex flow domain. We study an influence of wall shape on heat exchange and pressure drop in a 3D wavy channel.

2 Governing equations and solution procedure

We consider a low Mach number flow described by the continuity equation, the Navier-Stokes equations and the energy equation, which in the framework of an LES-IB approach are defined as:

$$\partial_t \bar{\rho} + \nabla \cdot (\bar{\rho}\widetilde{\mathbf{u}}) = 0 \tag{1}$$

$$\bar{\rho}\left(\partial_t \widetilde{\mathbf{u}} + (\widetilde{\mathbf{u}} \cdot \nabla)\widetilde{\mathbf{u}}\right) + \nabla \bar{p}\mathbf{I} = \nabla \cdot (\boldsymbol{\tau} + \boldsymbol{\tau}^{SGS}) + \mathbf{f}^{IB} \tag{2}$$

$$\bar{\rho} C_p \left(\partial_t \widetilde{T} + (\widetilde{\mathbf{u}} \cdot \nabla)\widetilde{T}\right) = \nabla \cdot \left((\kappa + \kappa^{SGS})\nabla T\right) + \mathrm{d}p_0/\mathrm{d}t + \mathrm{f}_T^{IB} \tag{3}$$

where the bar and tilde symbols denote filtered quantities [11]. The set of Eqs. (1)-(3) is complemented with the equation of state $p_0 = \bar{\rho} R \widetilde{T}$ with p_0 and R being the thermodynamic pressure and gas constant, respectively. In open flows with inlet/outlet boundaries p_0 is constant in space and time [10]. The variables $\mathbf{u}, \rho, p, T$ represent the velocity vector, density, pressure and temperature. The variable C_p is the heat capacity at constant pressure and the variables $\boldsymbol{\tau}$ and κ are the viscous stress tensor and thermal conductivity. The molecular viscosity (μ) is computed from the Sutherland law and $\kappa = \mu C_p/\mathrm{Pr}$, where Pr is the Prandtl equal to 0.71. The term $\boldsymbol{\tau}^{SGS} = 2\nu_t \mathbf{S}$ is the sub-filter tensor, where $\mathbf{S}$ is the rate of strain tensor of the resolved velocity field and ν_t is the sub-filter viscosity [12]. The sub-filter heat conductivity κ^{SGS} is modelled as $\kappa^{SGS} = \bar{\rho}\nu_t C_p/\mathrm{Pr}_t$, where Pr_t is the turbulent Prandtl number equal to 0.6. The source terms $\mathbf{f}^{IB}$ and f_T^{IB} originate from the IB method and their role is to act on a fluid in such a way as if there were a solid object immersed in the flow domain.

Sub-grid modelling. In this paper we apply the model of Vreman [12] in which the sub-filter viscosity is defined as:

$$\nu_t = C_v \sqrt{\frac{B_\beta}{\alpha_{ij}\alpha_i j}} \tag{4}$$

$$\alpha_{ij} = \frac{\partial \bar{u}_j}{\partial x_i} \quad , \quad \beta_{kl} = \Delta^2 \alpha_{mk}\alpha_{ml} \tag{5}$$

$$B_\beta = \beta_{11}\beta_{22} - \beta_{12}^2 + \beta_{11}\beta_{13} - \beta_{13}^2 + \beta_{22}\beta_{33} - \beta_{23}^2 \tag{6}$$

where the constant is equal $C_v = 0.025$. In the present implementation of the IB method the sub-grid viscosity is computed in all mesh points, also in these located in the solid-body regions.

2.1 Solution algorithm

The solution algorithm for Eqs. (1-3) is formulated in the framework of a projection method [13] for pressure-velocity coupling with a direct forcing approach for the IB method [14]. The time integration is based on a predictor-corrector approach (Adams-Bashforth/Adams Moulton) and the spatial discretisation is performed using 6th/5th order compact difference and WENO (Weighted Essentially Non-Oscilatory) schemes on half-staggered meshes [9, 10]. In the framework of the IB approach the solution algorithm is defined as follow.

Predictor step. Generally, we assume that the time-step (Δt) can vary as the flow velocity changes in the successive time-steps, $..., n-1, n, n+1, ...$ With this assumption the 2nd order Adams-Bashforth method is given as:

$$\frac{\bar{\rho}\widetilde{\mathbf{u}}^* - \bar{\rho}\widetilde{\mathbf{u}}^n}{\Delta t^n} = \underbrace{\left(1 + \frac{\Delta t^n}{2\Delta t^{n-1}}\right)\mathrm{Res}(\widetilde{\mathbf{u}}^n) - \frac{\Delta t^n}{2\Delta^{n-1}}\mathrm{Res}(\widetilde{\mathbf{u}}^{n-1}) - \nabla \bar{p}^n \mathbf{I}}_{\mathrm{RHS}_u} + \mathbf{f}^{IB} \tag{7}$$

$$\frac{\widetilde{T}_i^* - \widetilde{T}_i^n}{\Delta t^n} = \underbrace{\left(1 + \frac{\Delta t^n}{2\Delta t^{n-1}}\right)\mathrm{Res}(\widetilde{T}^n) - \frac{\Delta t^n}{2\Delta^{n-1}}\mathrm{Res}(\widetilde{T}^{n-1})}_{\mathrm{RHS}_T} + \frac{1}{\bar{\rho} C_p}\mathrm{f}_T^{IB} \tag{8}$$

where $\mathrm{Res}(\mathbf{u})$, $\mathrm{Res}(T)$ represents the convection and diffusion terms of the Nevier-Stokes and energy equations. The formulas for the source terms $\mathbf{f}^{IB}$ and f_T^{IB} are discussed latter. The RHS_u and RHS_T represent the spatial terms from Eq. (2) and Eq. (3). The velocity field u_i^* computed from Eq. (7) does not fulfill the continuity equation (i.e. $\bar{\rho}_t + \nabla \cdot (\bar{\rho}\tilde{u}^*) \neq 0$) and according to the projection method (see [13] or any other book on CFD) it must be corrected using the gradients of pressure correction (p') according to the following formula:

$$\bar{\rho}\widetilde{\mathbf{u}}^{**} = \bar{\rho}\widetilde{\mathbf{u}}^{*} - \Delta t^n \nabla p' \mathbf{I} \tag{9}$$

where p' is computed from the Poisson equation:

$$\nabla \cdot (\nabla p' \mathbf{I}) = \frac{1}{\Delta t^n} \left[\nabla \cdot (\bar{\rho}\widetilde{\mathbf{u}}^{*}) + \bar{\rho}_t^* \right] \tag{10}$$

resulting from the condition $\bar{\rho}_t + \nabla \cdot (\bar{\rho}\widetilde{\mathbf{u}}^{**}) = 0$. The density is computed from the equation of state $p_0 = \bar{\rho}^* R \widetilde{T}^*$ and its time derivative needed in (10) is disrcretized using 2nd order formula

$$\bar{\rho}_t^* = \frac{\left[(\Delta t^n + \Delta t^{n-1})^2 - (\Delta t^n)^2 \right] \bar{\rho}^* - (\Delta t^n + \Delta t^{n-1})^2 \bar{\rho}^n + (\Delta t^n)^2 \bar{\rho}^{n-1}}{\Delta t^n \Delta t^{n-1} (\Delta t^n + \Delta t^{n-1})} \tag{11}$$

Corrector step. The 2nd order Adams-Moulton method is defined as:

$$\frac{\bar{\rho}\widetilde{\mathbf{u}}^{*} - \bar{\rho}\widetilde{\mathbf{u}}^{n}}{\Delta t^n} = \underbrace{\frac{1}{2}(\mathrm{Res}(\widetilde{\mathbf{u}}^{**}) + \mathrm{Res}(\widetilde{\mathbf{u}}^{n})) - \nabla \bar{p}^n \mathbf{I}}_{\mathrm{RHS}_u} + \mathbf{f}_i^{IBM} \tag{12}$$

$$\frac{\widetilde{T}^{n+1} - \widetilde{T}^{n}}{\Delta t^n} = \underbrace{\frac{1}{2}(\mathrm{Res}(\widetilde{T}^{**}) + \mathrm{Res}(\widetilde{T}^{n}))}_{\mathrm{RHS}_T} + \frac{1}{\bar{\rho} C_p} \mathrm{f}_T^{IBM} \tag{13}$$

Again, the velocity field $\widetilde{\mathbf{u}}^*$ does not fulfill the continuity equation and its correction is defined as:

$$\bar{\rho}\widetilde{\mathbf{u}}^{n+1} = \bar{\rho}\widetilde{\mathbf{u}}^{*} - \Delta t^n \nabla p' \mathbf{I} \tag{14}$$

The equation $\bar{\rho}_t + \nabla \cdot (\bar{\rho}\widetilde{\mathbf{u}}^{n+1}) = 0$ leads to the Poisson equation (10). Its solution allows us to correct the velocity using (14) and to update the pressure field as:

$$p^{n+1} = p^n + p' \tag{15}$$

The density is computed from $p_0 = \bar{\rho}^* R \widetilde{T}^{n+1}$ and the next time step begins.

IB source term. Assuming a stationary wall with a given wall temperature the IB source terms are defined in terms of the phase-indicator function $\mathrm{H}(\mathbf{x})$ as:

$$\mathbf{f}^{IB} = \mathrm{H}(\mathbf{x}) \times \mathrm{RHS}_u(\mathbf{x}); \quad \mathrm{f}_T^{IB} = \mathrm{H}(\mathbf{x}) \times \mathrm{RHS}_T(\mathbf{x}); \text{ with } \mathrm{H}(\mathbf{x}) = \begin{cases} -1 & \text{for } \mathbf{x} \in \Omega_b \\ 0 & \text{otherwise} \end{cases} \tag{16}$$

where Ω_b denotes the solid body embedded in the computational domain. It is worth nothing that the source terms presented in the above forms are only needed to formally express an impact of IB on the flow domain. In practice, with the explicit time integration method the terms $\mathbf{f}^{IB}$ and f_T^{IB} are not computed and the IB method reduces to substituting $\widetilde{u} = u_{\Omega_b}$ and $\widetilde{T} = T_{\Omega_b}$ for $\mathbf{x} \in \Omega_b$, and to calculating the velocity and temperature near the solid boundaries.

2.2 Near boundary interpolation

In the direct forcing IB method the velocity and temperature in the grid nodes inside the solid objects are set equal to the velocity and temperature of the object, whereas their calculation on the fluid side requires

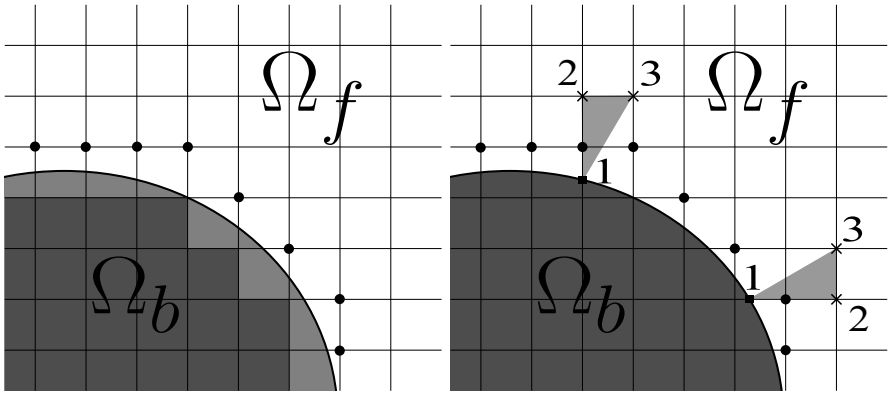

Figure 1: Stepwise approach (left) and near boundary interpolation method (right).

a special treatment. There are two approaches schematically shown in Fig. 1. In the first approach, the so-called stepwise, the boundary of the solid body is determined by a computational mesh. In the nodes located at $\mathbf{x} \in \Omega_b$ we simply put $\widetilde{u} = u_b^{\Omega}$ and $\widetilde{T} = T_b^{\Omega}$, whereas outside of Ω_b the values in the direct vicinity of the boundary (bold nodes) are computed from the governing equations as in every other node at $\mathbf{x} \in \Omega_f$. It is easy to recognize that in this approach the solid boundaries is 'seen' as if they had the stepwise shape (see dark grey colour in Fig. 1 on the left side). The denser the mesh the more accurate is representation of the real shape of the solid. In the second, more accurate approach, in the nodes lying near of the solid the values of the velocity and temperature are interpolated based on the real location of the solid boundary and the values in surrounding nodes on the fluid side (crosses in Fig. 1 on the right). In the present work we apply this approach and use an interpolation formula proposed in [15] given as:

$$\phi = b_1 + b_2 x + b_3 y \tag{17}$$

for which the coefficient b_1, b_2 and b_3 can be computed solving the system of equations:

$$\begin{bmatrix} b_1 \\ b_2 \\ b_3 \end{bmatrix} = \begin{bmatrix} 1 & x_1 & y_1 \\ 1 & x_2 & y_2 \\ 1 & x_3 & y_3 \end{bmatrix}^{-1} \begin{bmatrix} \phi_1 \\ \phi_2 \\ \phi_3 \end{bmatrix} \tag{18}$$

where x_i and ϕ_i are the values of the velocity and temperature in the locations 1, 2 and 3. Extension of the above interpolation method to 3D cases is straightforward.

3 Results

3.1 Test computations: accuracy and stability

The test computations have been performed for two cases: (i) 2D laminar flow around a cylinder; (ii) 3D turbulent flow around a sphere. The former test case had to verify accuracy of the proposed solution procedure and the latter its stability in simple 3D configuration. The computational meshes consisted of 128×192 and $128 \times 192 \times 128$ nodes compacted such that in the vicinity of the solid body (and inside) the cell sizes were equal to $1/30$ of the diameter of the cylinder or sphere, D. The computational domains were $10D \times 15D$ and $10D \times 15D \times 10D$. The uniform velocity ($U_{in}$) and temperature ($T_{in}$) were assumed at the inlet. The computations were performed for the Reynolds numbers $\mathrm{Re} = U_{in}D/\nu$ equal to 40 for the cylinder and 3700 for the sphere. The temperatures of the objects were equal to $2T_{in}$ and $5T_{in}$, respectively. The solution procedure stared from the zero velocity field everywhere in the domains and with the assumed temperatures of the solids and T_{in} elswhere. The computations continued until the steady state had been reached for 2D case or until the fully turbulent flow had developed in 3D case. Figure 2 shows the temperature contours around the cylinder and the profiles of temperature in selected locations behind the cylinder. The results are compared with the solution obtained using ANSYS Fluent code with body fitted mesh with

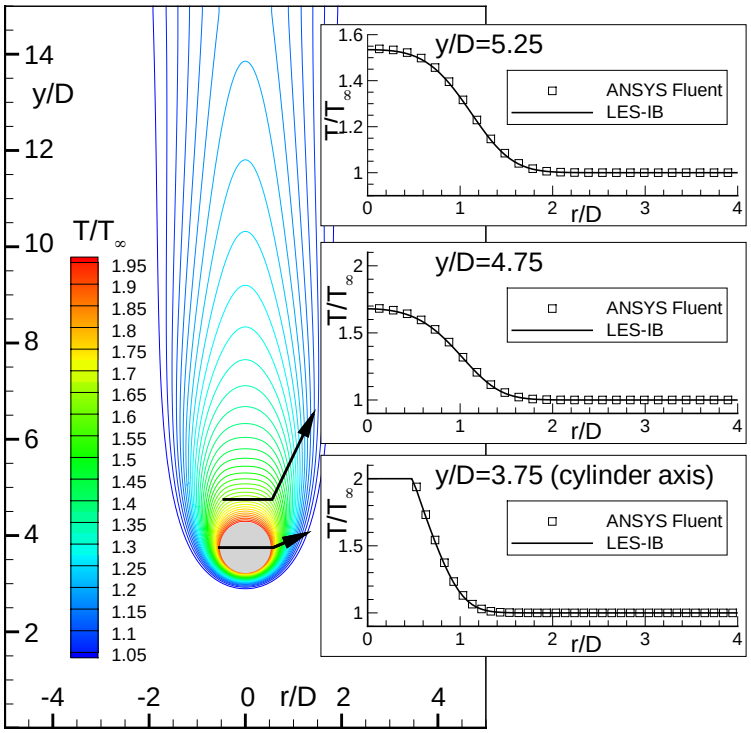

Figure 2: Laminar flow around 2D cylinder.

the cell sizes near the solid objects similar as in the IB method. It can be seen that the agreement of the results is excellent. Both the maxima of the temperature and its radial distribution are predicted very accurately. Figure 3 shows 3D iso-surfaces of the temperature, vorticity module and Q-parameter: $Q = 1/2(S_{ij}S_{ij} - \Omega_{ij}\Omega_{ij})$ where S_{ij} and Ω_{ij} are symmetrical and anti-symmetrical parts of the velocity gradient tensor. Careful inspection of flow regions near the sphere did not reveal any suspicious oscillations or other signs of instabilities (eg. temperature overshoots). Thus, one may conclude that the formulated algorithm is very accurate and stable.

3.2 Flow in a channel with a wavy wall

An efficient method of intensifying the heat exchange in channels is to apply walls with wavy shapes. From one side it increases an effective area of the heat transfer, and from the other it intensifies a mixing (turbulence). In this work we assume a sinusoidal wall with two control parameters, amplitude (A) and frequency (f). One should be aware that alteration of these parameters change not only the heat transfer process but also the flow behaviour, among others a pressure drop Δp along the channel. Knowledge of Δp enables to estimate the power ($\mathcal{P}$) needed to force the flow at assumed flow rate (Q), $\mathcal{P} = \Delta p \times Q$. The larger waviness of the flow the bigger Δp is, hence, we will analyzed the impact of A and f on both the temperature field and Δp.

The computational domain is shown in Fig. 4 with the location of the wall at: $A\sin(\omega y f)$, with $\omega = 2\pi/L_y$. The length of the domain in the streamwise direction is equal to $L_y/h = 4\pi$, the height of the channel is equal to $L_x/h = 2$ and the spanewise size is equal to $L_z/h = \pi$, where h is the half channel height. The periodic boundary conditions are applied in the spanewise direction. The lower wall is modelled using the IB method and the upper wall is treated in the classical way. The temperature of the walls are $T_l = 2T_{in}$ and $T_u = T_{in}$. The Reynolds numbers based on the the friction velocity $u_\tau = \sqrt{\nu \partial u/\partial y|_{y=h}}$, h and the kinematic viscosity at T_{in} is equal to $\mathrm{Re}_\tau = 300$. The computations were performed using three different meshes, their parameters (the node numbers and characteristic cell sizes) are shown in Table 1. Near the upper wall the nodes are compacted using the polynomial stretching function such that $\Delta y+ = \Delta(yu_\tau/\nu) < 1$.

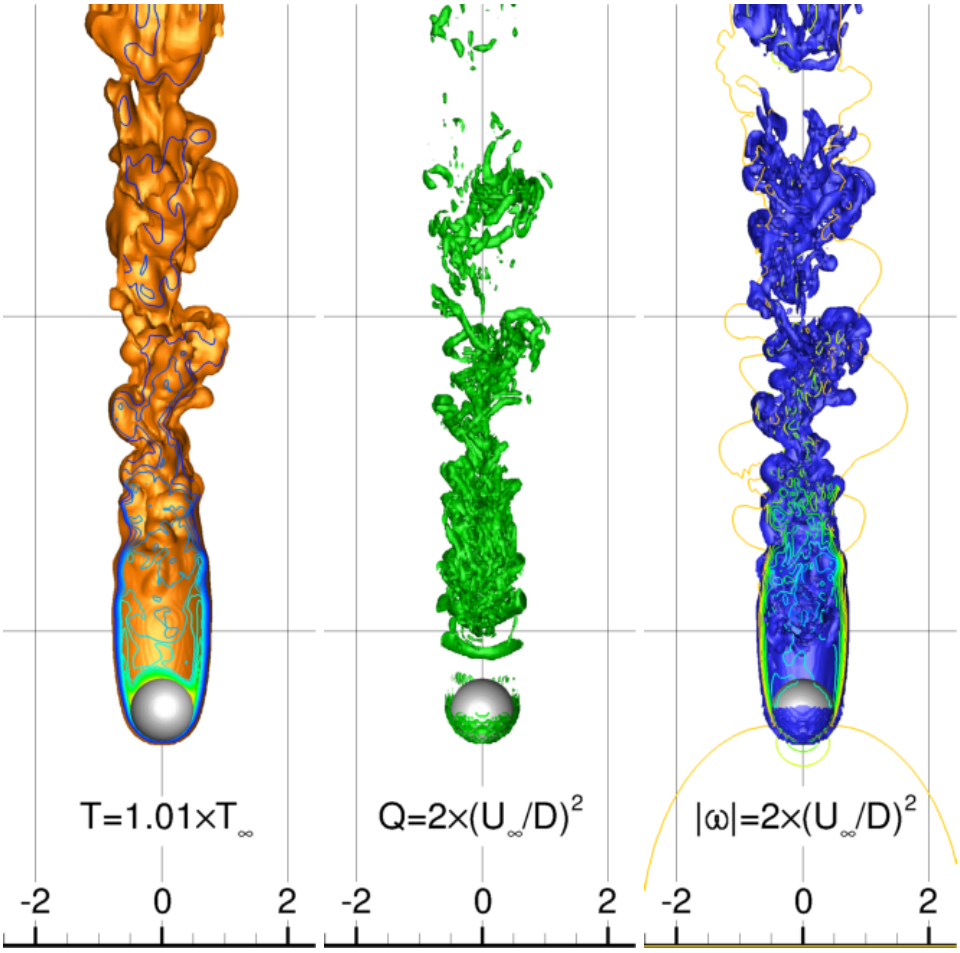

Figure 3: Turbulent flow around sphere.

3.2.1 Simulation results

Table 2 shows the parameters of all analyzed cases. The accuracy of the obtained solutions was verified in the test computations for $\mathrm{Re}_\tau = 10$ with $A = 0.25$ and $f = 6$ for which the flow remained laminar (Case 1 in Table 2). The IB solutions were compared with the results obtained using ANSYS Fluent code and it was found that in every spatial location the present results agreed almost perfectly. It is believed that the same level of accuracy is obtained in turbulent regimes. A sample solution obtained for the Case F6A25 is presented in Fig. 4. It shows instantaneous iso-surfaces of the Q-parameter ($Q = 2500$) and temperature contours which clearly present the turbulent flow behaviour. Detailed analysis of the contours of temperature, velocity and sub-grid viscosity in the region of the trough and top showed that the contours are smooth and the sub-filter viscosity vanishes in the solid region. The fact that $\nu_t \approx 0$ in Ω_b most likely results from a basic assumption of the model of Vreman, i.e. the region Ω_b is 'seen' by the model as not turbulent flow region. Figure 5 shows the evolution of the Nusselt number and Δp in the function of A and f obtained on the mesh C. We notev that on the meshes A and B the obtained solutions were very similar and small differences had only quantitative character. It can be seen that compared to the straight channel (case F0A00) the waviness significantly changes the flow character. One may observe that for $f = 4$ and $f = 6$ starting from the second top wave location the maxima of the Nusselt number remain at the same level and they depend only on the amplitude of the waves. The larger are the values of A the stronger variation of the Nusselt number is observed. On the other hand, the pressure did not exhibit such a strong dependence on A and its variations along the channel are smooth.

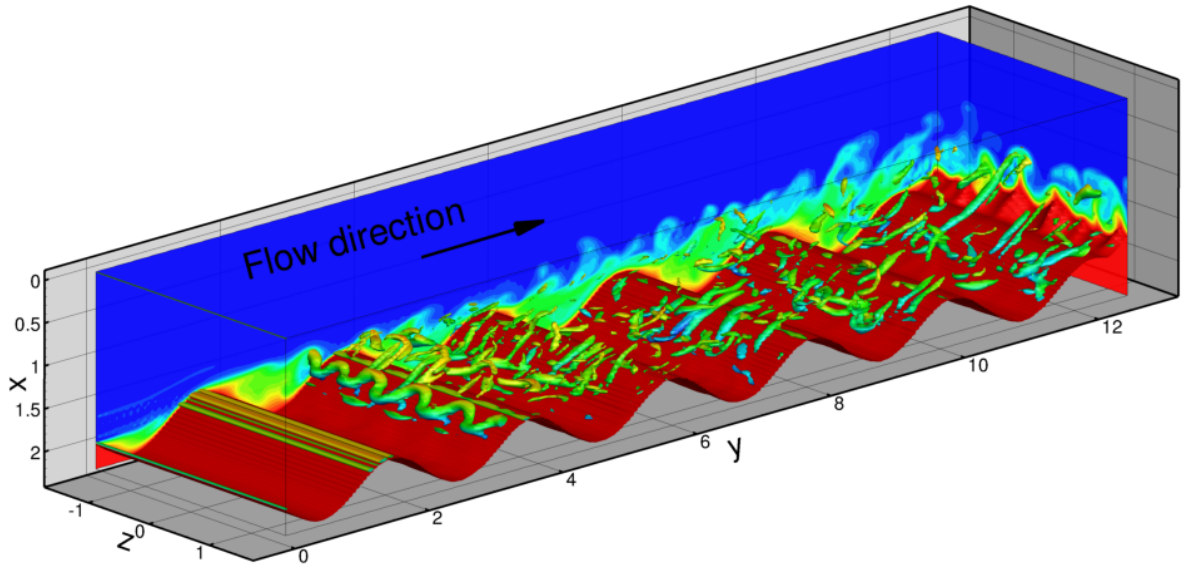

Figure 4: Instantaneous iso-surface of Q-parameter and temperature contours for the case F6A25.

Table 1: Parameters of the computational meshes for the flow in wavy channel. Maximum and minimum Δx^+ sizes for each configuration are expressed as: Δx^+_{min},Δx^+_{max}.

Mesh	$N_x \times N_y \times N_z$	$N_{x,\text{uni.}}$ in $x-$range	Δy^+	Δz^+	$\Delta x^+_{uni.}$, Δx^+_{min}, Δx^+_{max}
A	$160 \times 240 \times 64$	32 in $x \geq 1.7$			$5.806, 0.998, 5.806$
B	$176 \times 240 \times 64$	48 in $x \geq 1.7$	15.77	14.96	$3.829, 1.000, 5.944$
C	$192 \times 240 \times 64$	64 in $x \geq 1.7$			$2.857, 0.978, 6.425$

4 Conclusions

The paper presented the solution algorithm for Large Eddy Simulation - Immersed Boundary method for variable density flows analyzed in a framework of the low Mach number approximation with large density/temperature variations. The test computations performed for laminar flow regimes and comparisons with the results obtained form the simulations performed using a classical body-fitted mesh proved the high accuracy of the proposed technique. The computations carried out for turbulent flows around the sphere and in the channel with the wavy wall showed that it can be used also in complex flow domains. In all the cases the obtained solutions were stable and exhibited expected behaviour.

Acknowledgments

The investigation was supported by Polish National Science Center under Grant no. DEC-2012/07/B/ST8/03791. The computations were performed using an infrastructure of PL-Grid (Poland).

References

[1] J. Fang, M. Diebold, C. Higgins, M.B. Parlange. Towards oscillation-free implementation of the immersed boundary method with spectral-like methods. *Journal of Computational Physics*, 230:8179-8191, 2011.

[2] P.J.S.A. Ferreira de Sousa, J.C.F. Pereira, J.J. Allen. Two-dimensional compact finite difference immersed boundary method. *International Journal for Numerical Methods in Fluids*, 65:609-624, 2011.

Table 2: Test cases parameters for the flow in wavy channel.

Case	Freq.	Amplitude	Case	Freq.	Amplitude.	Case	Freq.	Amplitude
F2A05	2	0.05	F4A05	4	0.05	F6A05	6	0.05
F2A10	2	0.10	F4A10	4	0.10	F6A10	6	0.10
F2A15	2	0.15	F4A15	4	0.15	F6A15	6	0.15
F2A20	2	0.20	F4A20	4	0.20	F6A20	6	0.20
F2A25	2	0.25	F4A25	4	0.25	F6A25	6	0.25

[3] E. A. Fadlun, R. Verzicco, P. Orlandi, J. Mohd-Yusof. Combined immersed-boundary finite-difference methods for three-dimensional complex flow simulations. *Journal of Computational Physics*, 161:35-60, 2000.

[4] E. Balaras. Modeling complex boundaries using an external force field on fixed Cartesian grids in large-

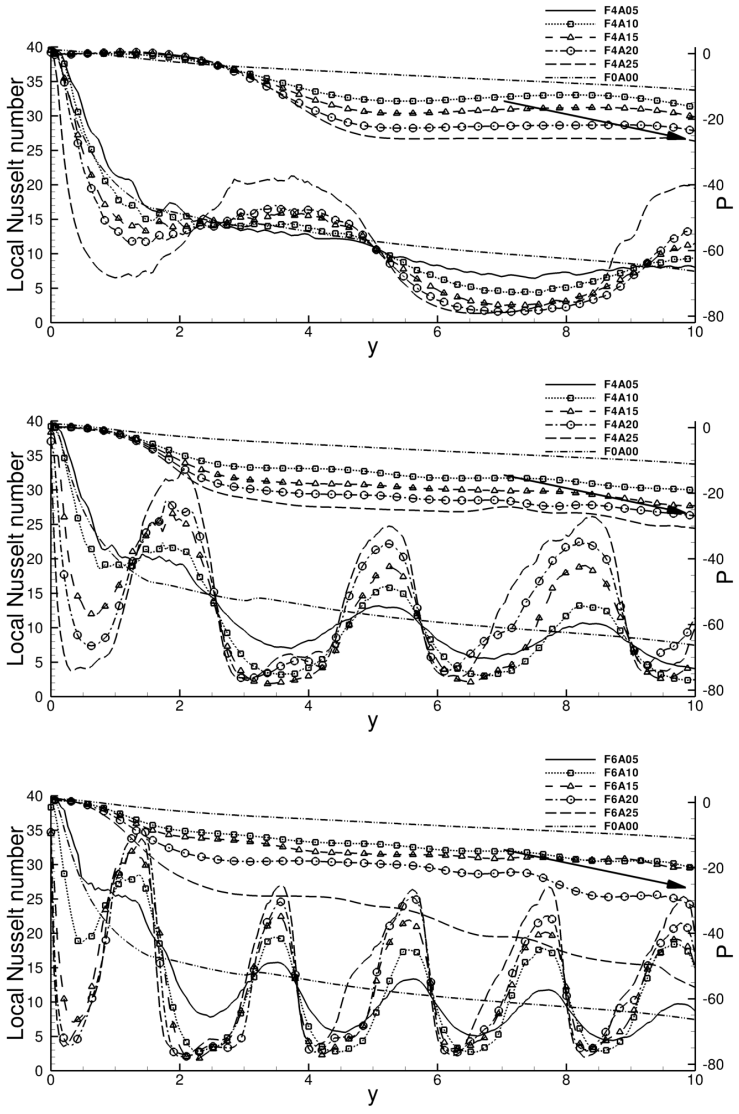

Figure 5: Local Nusselt number and pressure drop for the cases with $f = 2, 4, 6$ and various amplitudes.

eddy simulations. *Computers and Fluids*, 33:375-404, 2004.
[5] D.G.E. Grigoriadis, J.G. Bartzis, A. Goulas. Efficient treatment of complex geometries for large eddy simulations of turbulent flows. *Computers and Fluids*, 33:201-222, 2004.
[6] Gautier, R., Laizet, S., Lamballais, E., A DNS study of jet control with microjets using an alternating direction forcing strategy *International Journal of Computational Fluid Dynamics* 28:393-410, 2014.
[7] Gronskins, A., Artana, G. A simple and efficient direct forcing immersed boundary method combined with a high order compact scheme for simulating flows with moving rigid boundaries Computers ans Fluids 124:86–104, 2016.
[8] W. Ren, C. Shu, W. Yang. An efficient immersed boundary method for thermal flow problems with heat flux boundary conditions *International Journal of Heat and Mass Transfer*, 64:694-705, 2013.
[9] A. Tyliszczak. A high-order compact difference algorithm for half-staggered grids for laminar and turbulent incompressible flows. *Journal of Computational Physics*, 276:438-467, 2014.
[10] A. Tyliszczak. High-order compact difference algorithm on half-staggered meshes for low Mach number flows. *Computers and Fluids*, 127:131-145, 2016.
[11] B.J. Geurts. Elements of Direct and Large-Eddy Simulation. *Edwards Publishing, Philadelphia, USA*, 2004.
[12] A.W. Vreman. An eddy-viscosity subgrid-scale model for turbulent shear flow: Algebraic theory and applications. *Physics of Fluids*, 16:3670?3681, 2004.
[13] C.A.J. Fletcher. Computational Techniques for Fluid Dynamics. *Springer-Verlag*, Berlin, 1991.
[14] R. Mittal, G. Iaccarino. Immersed Boundary Methods. *Annual Review of Fluid Mechanics*, 37:239-261, 2005.
[15] J. Yang, E. Balaras. An embedded-boundary formulation for large-eddy simulation of turbulent flows interacting with moving boundaries *Journal of Computational Physics*, 215:12-40, 2006